Submitted to the proceedings of the EUMETSAT Meteorological Satellite Conference & 19th American Meteorological Society (AMS) Satellite Meteorology, Oceanography, and Climatology Conference, held in Vienna, Austria, 16-20 September 2013.

HIGH FREQUENCY MEASUREMENT OF SUSPENDED SEDIMENTS AND COCCOLITHOPHORES IN EUROPEAN AND AFRICAN COASTAL WATERS FROM THE GEOSTATIONARY SEVIRI SENSOR

Quinten Vanhellemont[1], Griet Neukermans[2], and Kevin Ruddick[1]

[1] Royal Belgian Institute for Natural Sciences (RBINS), Direction Natural Environment, 100 Gulledelle, 1200 Brussels, Belgium. e-mail: quinten.vanhellemont@mumm.ac.be

[2] Marine Physical Laboratory, Scripps Institution of Oceanography, University of California, San Diego, La Jolla, CA 92093-0238, USA.

Abstract

In this study, the processing of SEVIRI data for marine applications developed for the southern North Sea by Neukermans et al. (2012, 2009) is generalized. The updated processing can be applied to any region in SEVIRI's full viewing disk (centred on 0°N, 0°E) where the marine signal is sufficiently high (turbidity > ~1 FNU). Rayleigh and aerosol look-up-tables now account for all possible viewing and sun geometries. Parameters that can be derived from marine reflectance in a broad red band (560-710 nm) such as turbidity and suspended matter concentration can be studied at high temporal resolution. Marine reflectance from SEVIRI compared well with marine reflectance from MODIS-Aqua for several European and African coastal waters. The capabilities of high frequency imagery are well illustrated. For example, cloud clearing capabilities show improved coverage of a coccolithophore bloom and short-term changes in turbid coastal waters are observed on cloud-free days.

1. Introduction

Suspended particulate matter concentrations (SPM) have been studied using ocean colour sensors (such as SeaWiFS, MODIS, and MERIS) for over a decade (e.g. Blondeau-Patissier et al., 2004; Nechad et al., 2003; van der Woerd and Pasterkamp, 2004). These sensors are installed on polar orbiting satellites and provide global coverage every couple of days. Unfortunately, data availability is often strongly reduced due to cloud cover. The temporal resolution of imagery from polar orbiters is too low to study sub-diurnal SPM variability, e.g. resuspension during a tidal cycle. Geostationary orbits offer a much higher temporal resolution that allows the study of such high frequency processes. The Korean Geostationary Ocean Colour Imager (GOCI) is currently the only dedicated ocean colour sensor on a geostationary platform. GOCI provides hourly imagery during daylight of the waters around the Korean peninsula with a band configuration similar to SeaWiFS and a spatial resolution of 500 m (Ryu et al., 2012). Both ESA and NASA are examining possibilities of launching geostationary ocean colour sensors that covers European and North American waters (IOCCG, 2012). The Spinning Enhanced Visible and InfraRed Imager (SEVIRI), a geostationary meteorological sensor, has been successfully used to determine SPM in the southern North Sea (Neukermans et al., 2012, 2009). The high temporal frequency of the imagery (every 15 minutes) from its broad red band (560-710 nm) allows the study of changes in SPM on cloud-free days (Neukermans et al., 2012). On days with scattered and moving clouds, multiple observations can be combined into a daily composite. In this paper we describe updates to the SEVIRI processing routines by Neukermans et al. (2012, 2009), hereafter termed "SP2012", for processing of other regions in the SEVIRI field of view. Examples for several turbid coastal waters and an offshore coccolithophore bloom are shown.

2. Methods

A brief summary of SP2012 is given in paragraph 2.1. Full details can be found in Neukermans et al. (2012, 2009). The updates for the processing, hereafter termed 'SP2013', are described in paragraphs 2.2-2.5. The MATLAB routines of Neukermans et al. (2012, 2009) were ported to IDL and split into modules.

2.1 Brief overview of SP2012

The VIS06 (560-710 nm) and VIS08 (740-880 nm) bands are used to retrieve marine reflectance in the VIS06 band. The VIS08 band is used for the estimation of aerosol reflectance. First, the top of atmosphere reflectances (ρ_{TOA}) are corrected for gas absorption and Rayleigh scattering and transmittance to give Rayleigh and gas corrected reflectances (ρ_C). Rayleigh reflectance and transmittances are computed by 6SV (Kotchenova et al., 2006) and stored in look-up tables (LUTs) as function of sun-sensor geometry and wind speed. Two assumptions are made for the atmospheric correction: 1) the ratio of marine reflectances in the VIS06 and VIS08 bands, σ, is a constant equal to 6.09 and 2) the ratio of aerosol reflectances in those bands, ε ($= \rho_a^{VIS06}/\rho_a^{VIS08}$), is spatially constant in the southern North Sea, but varies temporally. This ratio is computed from the ρ_c ratio over clear water pixels. The ratio of aerosol transmittances in both bands, γ ($= t_a^{VIS06}/t_a^{VIS08}$), is determined in a two step process. First, the aerosol reflectance is estimated by γ=1. The aerosol optical thickness, τ_a, is retrieved from a LUT, as function of geometry and ρ_a, and then the aerosol transmittance, t_a, is retrieved from a LUT, as function of geometry and τ_a. This gives a new estimate of γ and ρ_a, and the above steps are repeated to give the final τ_a and t_a.

2.2 Regionalisation

Full disk imagery is stored as 3712 lines by 3712 samples in unsigned 2-byte integers, with gain and offset values for calibration in the file's header. New regions are defined by geographical coordinates. A bounding box in the full disk is determined and the corresponding pixel ranges are stored for rapid cropping during the processing of the region. Ancillary data for each region include: 1) a land mask derived from the Global Self-consistent, Hierarchical, High-resolution Geography database (GSHHG), Wessel and Smith, 1996, and 2) a selection of clear water pixels (see next paragraph).

2.3 Clear water pixel selection

Clear water pixels are necessary for the estimation of the ratio of aerosol reflectances, ε, and are determined *a priori* for each region. In SP2012, a two-step clear water pixel selection was performed: First, predefined boxes of offshore clear water pixels were chosen and applied to a two year image archive. Next, clear water pixels were redefined as those pixels for which remotely sensed SPM was < 3 gm^{-3} at least 95% of the time. In SP2013, a MODIS-Aqua climatology (06/2002-07/2012) of remote sensing reflectance in the 645 nm band is used to determine clear waters with a region-specific threshold.

2.4 Cloud masking

Unrealistic persistent cloud features were found in the standard cloud mask (Lutz, 1999), influencing data availability and adding erroneous features to daily composites. Additionally, for some full disk data, the cloud mask file (CLM) was not available. SP2013 was therefore updated to work with and without the

CLM. Cloud free pixels over clear waters are needed for the aerosol correction. If the CLM is available it is used in this stage, and, if it is not available, a threshold on ρ_c of 10% is used on the predetermined clear water pixels. In both cases, the cloud mask on the final product is determined after the atmospheric correction, by applying a threshold of 85% on t_a^{VIS06}.

2.5 Look-up tables

In SP2012, the look up tables (LUTs) were set up for viewing and illumination geometries typical to the southern North Sea. For SP2013, three full sets of LUTs were generated using 6SV 1.1 (Kotchenova et al., 2006) using the relative spectral response of SEVIRI on MSG-1, MSG-2 and MSG-3. LUTs are generated for Rayleigh reflectance, ρ_r, and Rayleigh diffuse transmittances for sun-sea and sea-sensor paths (t_d and t_u), and for aerosol reflectance, ρ_a, and two way aerosol diffuse transmittance (t_{d+u}). Details of each LUT are given in Table 1. For computational reasons the aerosol LUTs are quite coarsely spaced.

Table 1 Details on spacing of the look up tables (LUTs) used in the SEVIRI processing.

LUT type	**Output parameters**	**Dimensions**
Rayleigh	ρ_r, t_d, t_u	37 relative azimuth angles (ϕ) 0-180°, every 5° 26 sun and viewing zenith angles (θ_s, θ_v): 0-68° every 4°, 70-80° every 2°, 81°, 82° 4 wind speeds: 0.001,5,10,15 ms^{-1}
Aerosol	ρ_a, t_{d+u}	14 relative azimuth angles (ϕ): 0,5,10,20,40,60,80,100,120,140,160,170,175,180° 13 sun and viewing zenith angles (θ_s, θ_v): 8,16,24,32,40,48,56,64,70,74,78,80° 3 optical thicknesses: 0.01, 0.5, 1.0

2.6 Comparison of SEVIRI and MODIS-Aqua marine reflectance

SP2012 processing has previously been validated with in situ measurements from buoys and MODIS-Aqua data, (Neukermans et al., 2012; Vanhellemont et al., 2013). For the study areas presented here no in situ measurements were available, and therefore marine reflectance from SP2013 is compared with MODIS-Aqua from processing versions R2012.0 (2009 data) and R2013.0 (2012 and 2013 data). Details of these processors can be found online: http://oceancolor.gsfc.nasa.gov/WIKI/OCReproc.html. Standard L2 MODIS products were acquired for each region and reprojected on the SEVIRI HRV grid. This grid has a 1x1 km ground sampling distance (GSD) at the SEVIRI sub-satellite point, and the spatial resolution increases with viewing zenith angle, θ_v (Figure 1). The spatial resolution of the VIS06 and VIS08 bands is 3x3 km at the SEVIRI sub-satellite point. When nadir-viewing, MODIS has a 1 km resolution, gradually worsening away from the swath center. The 645 nm band has a 250 m resolution but is resampled to 1 km in the standard processing. So when both instruments are nadir viewing (i.e. at SEVIRI's sub-satellite point), there are nine MODIS pixels to the SEVIRI pixel. The comparison between MODIS and SEVIRI reflectance data is affected by differences in spectral, radiometric and spatial

resolutions. Additional effects include the bidirectional reflectance distribution function (BRDF) of suspended sediments and geometric distortion of the imaged region. SP2013 data is smoothed using a 5 image temporal filter to reduce noise (Vanhellemont et al., 2013).

Figure 1 shows SEVIRI's field of view and viewing angle. The regions where data was compared with MODIS-Aqua are highlighted. The spatial resolution - as pixel diagonal in km - is estimated from the L1.5 geolocation.

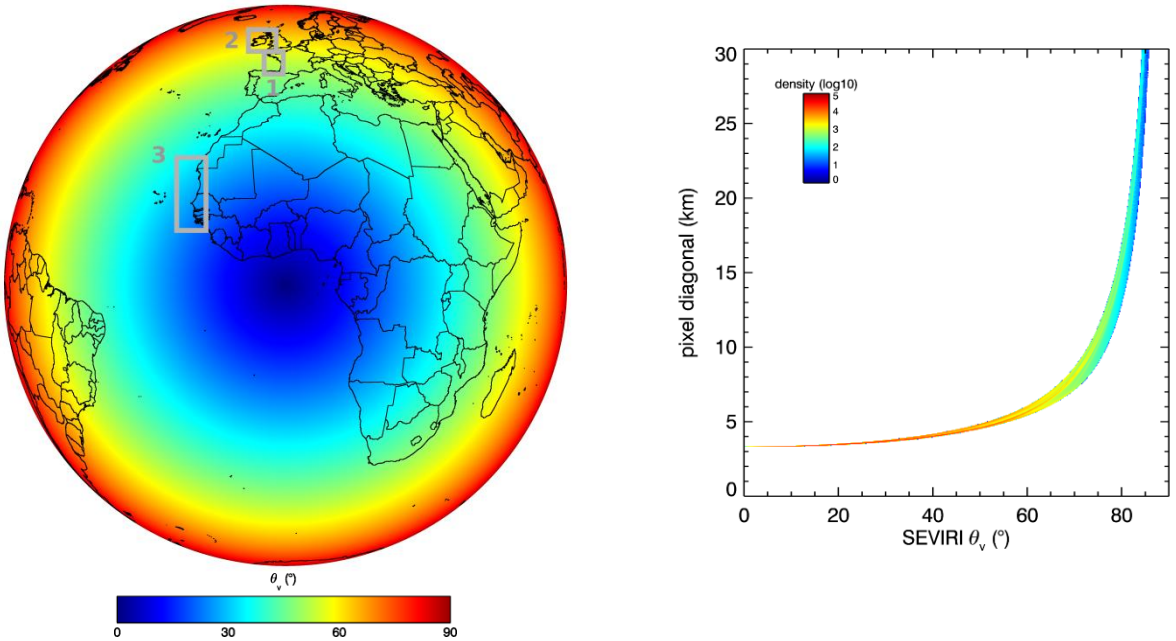

Figure 1 Left: Viewing zenith angle (θ_v) from SEVIRI-MSG at 0° E, with country borders drawn in black and test regions in grey: 1) Bay of Biscay, 2) Irish and Celtic Seas, and 3) Northwest African coast. Right: Pixel diagonal (km) as function of SEVIRI θ_v.

3. Results & Discussion

3.1 Bay of Biscay

Maps of SEVIRI marine reflectance for the Bay of Biscay (43°N, 49°N; 6°W, 0°E) are shown in Figure 2 and Figure 3. Turbid coastal waters around the Mont-Saint-Michel Bay (~48.5°N, 2°W), the Loire estuary (~47.2°N, 2.2°W), in the Pertuis d'Antioche strait (~46.3°N, 1.5°W), and the Gironde plume are clearly visible. In the more turbid waters SEVIRI underestimates reflectance with respect to MODIS. The main cause of this is probably the assumption of a constant ratio of marine reflectances in the VIS06 and VIS08 bands (σ), which is clearly invalid even for moderately turbid waters (see e.g. Figure 4.7 in Neukermans, 2012). The difference in masked data (white patches) is due to difference in cloud masking, more stringent quality control of the MODIS data using the level 2 flags, and because of the 5-image moving average filter applied to the SEVIRI data.

In Figure 3, a large offshore patch of increased reflectance is visible. This was identified as a bloom of coccolithophores, phytoplankton with calcium carbonate shells. Coccolithophores are known to be strong light scatterers because of their carbonate shells, and can be easily detected using remote sensing data (Balch et al., 1991). In fact, imagery from sensors such as Landsat/MSS, CZCS and AVHRR first illustrated the large extent of the coccolithophore blooms (Groom and Holligan, 1987; Holligan et al., 1983). Coccolithophores contribute strongly to offshore primary production, and by building their shells they consume CO_2 that will eventually be exported to the sea floor (Beaufort and Heussner, 2001; Harlay et al., 2010; Schmidt et al., 2013; Ziveri et al., 2000), contributing significantly to long-term carbon burial. However, their short-term and seasonal dynamics are not fully understood.

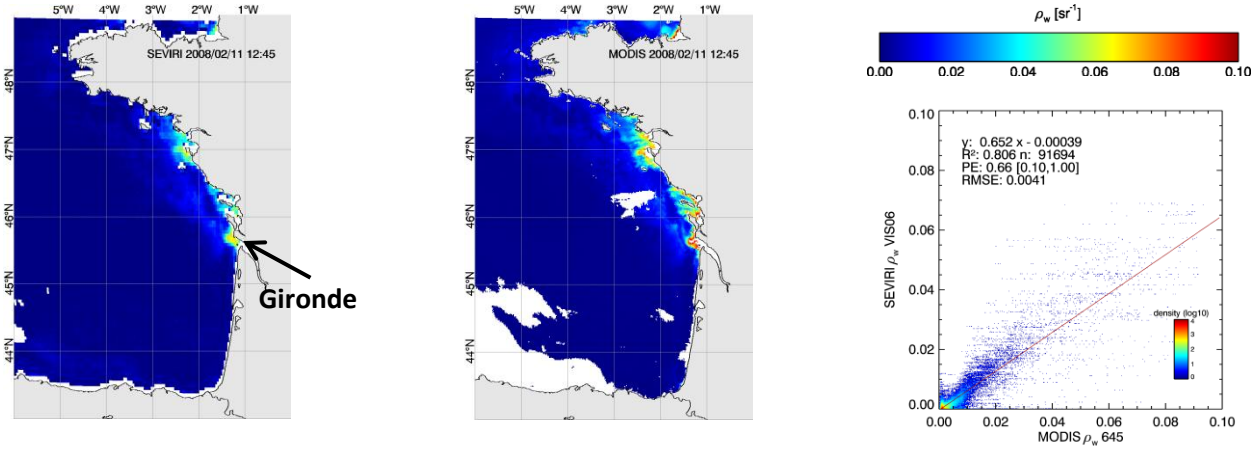

Figure 2 Marine reflectance from SEVIRI-MSG2 (left) and MODIS-Aqua (middle) on 2008-02-11 (12:45 UTC) for the Bay of Biscay, and a scatter plot comparing the two (right).

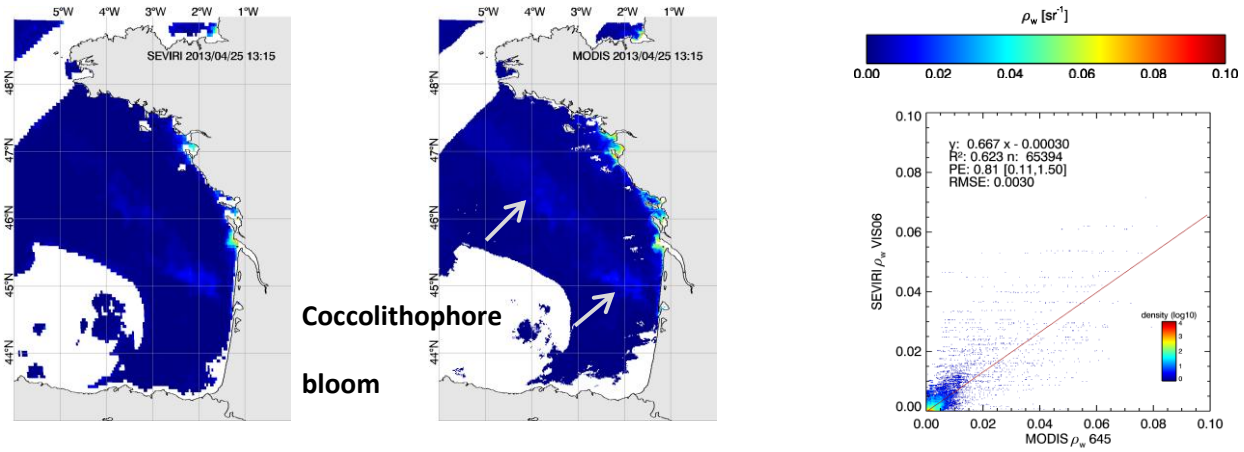

Figure 3 Marine reflectance from SEVIRI-MSG3 (left) and MODIS-Aqua (middle) on 2013-04-25 (13:15 UTC) for the Bay of Biscay, and a scatter plot comparing the two (right). A large offshore coccolithophore bloom is visible, located along the shelf break.

Figure 4 shows daily composites of SEVIRI marine reflectance and daily images of MODIS marine reflectance in the Bay of Biscay for several days in April 2013. Features of interest are the large offshore

coccolithophore bloom and the Gironde river plume. On the daily images from MODIS, much of the study area is obscured by clouds, and it is impossible to assess temporal dynamics. On cloudy days, a geostationary imager will be better able to observe and track coastal and offshore phenomena that are missed with a single image from polar orbiters (see also Neukermans, 2012; Ruddick et al., 2013, 2012). On cloud-free days, temporal changes can be detected (see Figure 5).

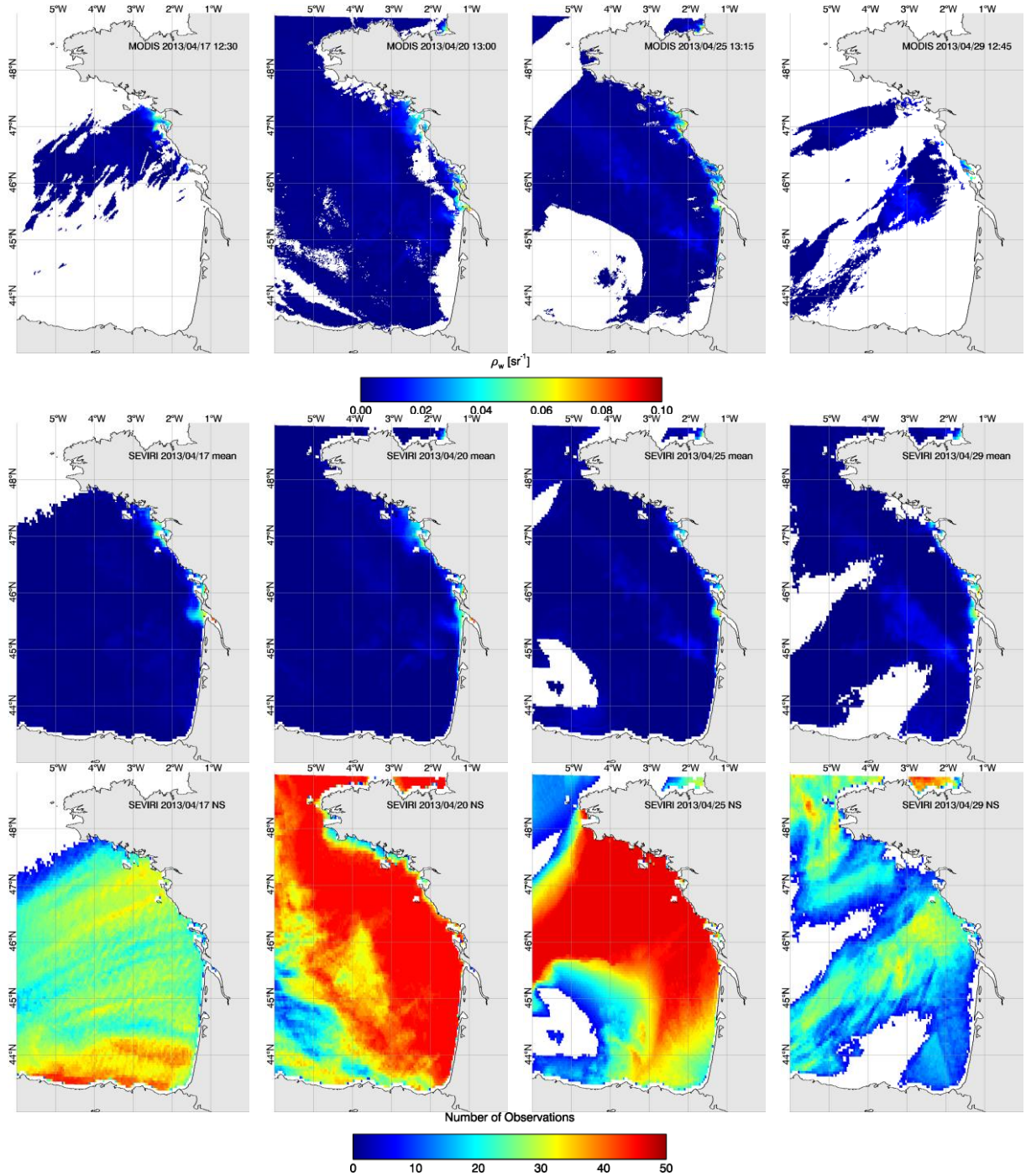

Figure 4 Daily mean marine reflectance from MODIS-Aqua (top) and SEVIRI-MSG3 (middle) and the number of SEVIRI observations (bottom) for the Gulf of Biscay on several days in April 2013.

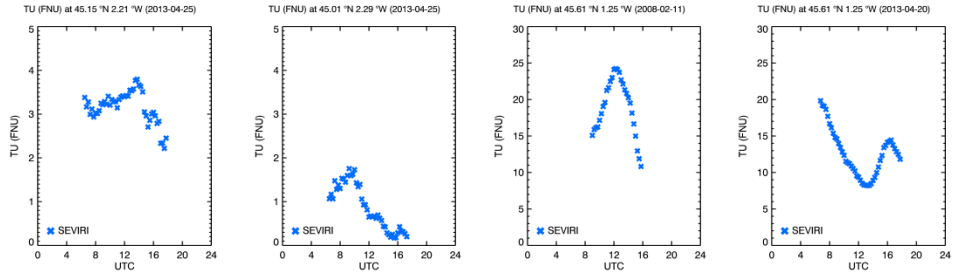

Figure 5 Time series of turbidity (using the algorithm of Nechad et al., 2009; Neukermans et al., 2012) derived from SEVIRI on MSG2 and MSG3, showing tidal variability of: a-b) two points in the coccolithophore bloom on 2013-04-25, and c-d) the turbid coastal water near the Gironde plume on 2008-02-11 (Low tide at ~12:50 UTC) and 2013-04-20 (High tide at ~12:10 UTC).

3.2 Irish and Celtic Seas

For the Irish and Celtic Seas (49°N-60°N, 12°W-2°W, Figure 6) the sensors are also in good agreement. Tidal currents are strong (> 1 ms^{-1}) in the Irish Sea, causing large semi-diurnal variation of turbidity (Weeks et al., 1993). Due to the frequent cloud cover in this region it is difficult to draw conclusions on temporal cycles by using data from MODIS-Aqua alone (Neil et al., 2012) and thus the potential of a geostationary sensor in this region is high. Because of the oblique viewing, the geometric distortions in the SEVIRI image are quite severe.

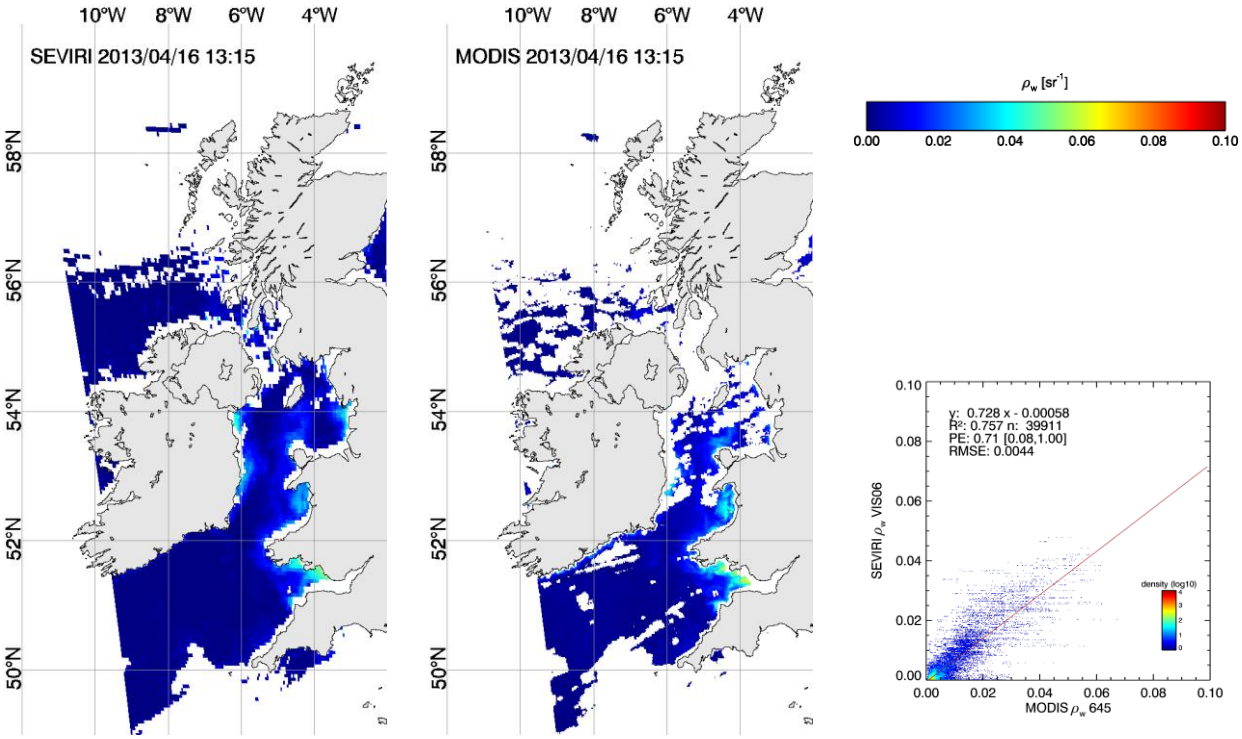

Figure 6 Marine reflectance from SEVIRI-MSG3 (left) and MODIS-Aqua (middle) on 2013-04-16 (13:15 UTC) for the Irish and Celtic seas, and a scatter plot comparing the two (right).

3.3 Northwest African coast

Turbid waters around the Northwest African coast (10°N - 22°N; 20°W - 15°W, Figure 7) include the shallow waters of the Banc D'Arguin National Park (~ 20°N, 17°W) where sand banks provide important breeding and foraging grounds for migratory birds (Wolff and Smit, 1990). Further South, turbid coastal waters are found where a number of large rivers enter the Atlantic Ocean in a region with extensive intertidal mudflats and mangroves (Anthony, 2004; Capo et al., 2006). A comparison of marine reflectance data from MODIS and SEVIRI on 14 April 2009 illustrates very good agreement between the sensors with $R^2 = 0.88$. The spatial resolution is less coarse here as this region is closer to the sub-satellite point. Time-series at two selected locations (11.81°N, 16.64°W and 19.60°N, 16.72°W) are given in Figure 8, showing the large high frequency variability in turbidity, up to a factor of two or more.

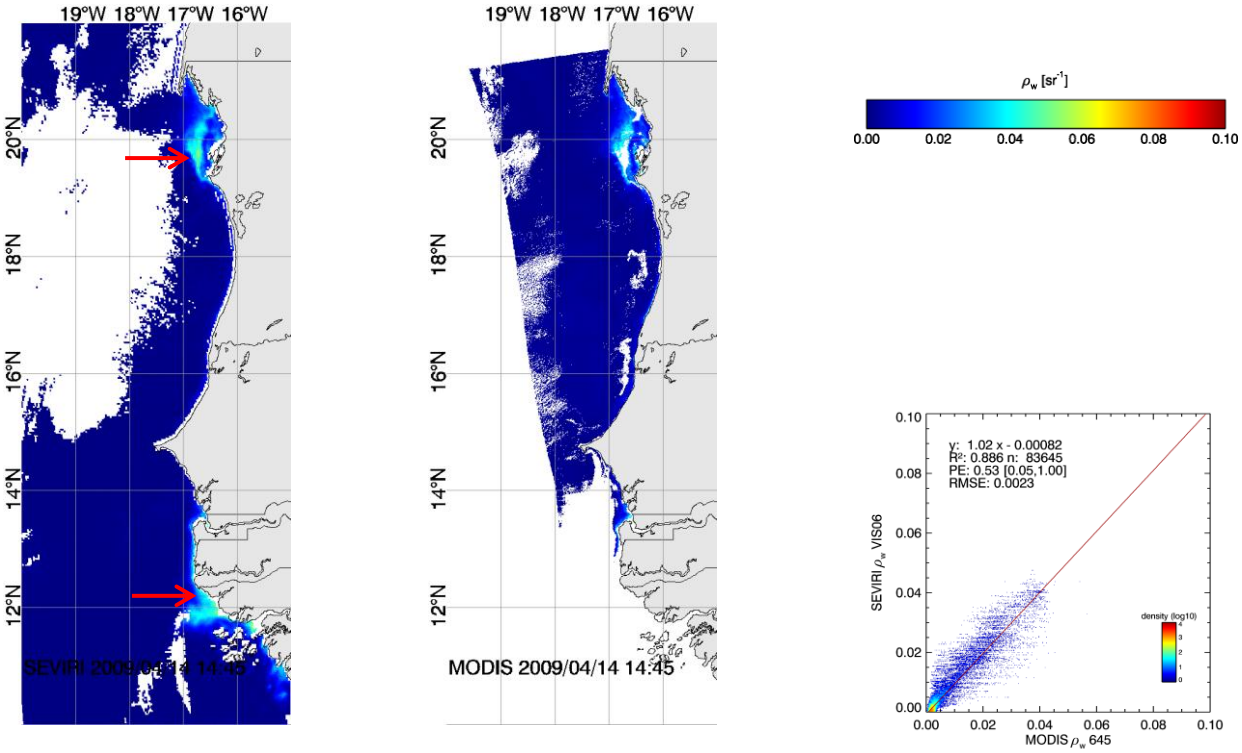

Figure 7 Marine reflectance from SEVIRI-MSG2 (left) and MODIS-Aqua (middle) on 2009-04-14 (14:45 UTC) for the north-west African coast, and a scatter plot comparing the two (right). The red arrows show the locations of the time-series in Figure **8**. Differences in masking are due to temporal averaging of SEVIRI data and the MODIS cloud and high glint flags.

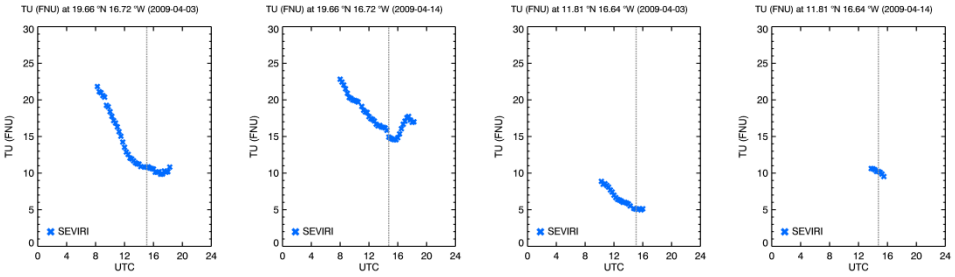

Figure 8 Turbidity variation derived from SEVIRI-MSG2 for two locations on the Northwest coast of Africa: a-b) Banc D'Arguin, c-d) Guinea-Bissau coast. The dashed grey line is the MODIS overpass time.

4. Conclusion

The SEVIRI processing for marine applications from Neukermans et al., (2012, 2009) has been generalized and successfully updated to process other regions in the full disk imagery. Marine reflectance products from the MODIS and SEVIRI sensors were in good agreement for each region. The advantages of a geostationary sensor are once more illustrated: variation over the day can be detected on days with clear skies, and on days with patchy cloud cover a strong increase of data coverage can be achieved with daily composites. The high value that could be provided by a future geostationary ocean colour sensor is demonstrated: Firstly for coastal waters, where short term processes such as tidal resuspension and river plumes are important; secondly for offshore waters, where huge coccolithophore blooms have high importance for the global carbon cycle.

Future prospects include processing of the full disk without cropping to given regions. The treatment of turbid waters in the atmospheric correction is currently based on the assumption of constant ratio of marine reflectance VIS06:VIS08. This should be improved since even for moderately turbid waters this relationship is clearly nonlinear. The effect of the bidirectional reflectance distribution function (BRDF) of marine particles can be large for specific combinations of sun and sensor zenith angles and the relative azimuthal angle (Vanhellemont et al., 2013) and has to be examined further. Similarly, in parts of the disk, sun glint is unavoidable and it has to be detected and masked.

Acknowledgements

This study was funded by the Belgian Science Policy Office (BELSPO) in the framework of the GEOCOLOUR project (contract SR/00/139). EUMETSAT and the Royal Meteorological Institute of Belgium (RMI) are thanked for the SEVIRI data, and NASA/OBPG for the MODIS data.

5. References

Anthony, E.J., 2004. Sediment dynamics and morphological stability of estuarine mangrove swamps in Sherbro Bay, West Africa. Mar. Geol. 208, 207–224.

Balch, W.M., Holligan, P.M., Ackleson, S.G., Voss, K.J., 1991. Biological and optical properties of mesoscale coccolithophore blooms in the Gulf of Maine. Limnol. Ocean. 36, 629–643.

Beaufort, L., Heussner, S., 2001. Seasonal dynamics of calcareous nannoplankton on a West European continental margin: the Bay of Biscay. Mar. Micropaleontol. 43, 27–55.

Blondeau-Patissier, D., Tilstone, G., Martinez-Vicente, V., Moore, G., 2004. Comparison of bio-physical marine products from SeaWiFS, MODIS and a bio-optical model with in situ measurements from Northern European waters. J. Opt. Pure Appl. Opt. 6, 875.

Capo, S., Sottolichio, A., Brenon, I., Castaing, P., Ferry, L., 2006. Morphology, hydrography and sediment dynamics in a mangrove estuary: the Konkoure estuary, Guinea. Mar. Geol. 230, 199–215.

Groom, S., Holligan, P., 1987. Remote sensing of coccolithophore blooms. Adv. Space Res. 7, 73–78.

Harlay, J., Borges, A., Van Der Zee, C., Delille, B., Godoi, R.H.M., Schiettecatte, L.-S., Roevros, N., Aerts, K., Lapernat, P.-E., Rebreanu, L., others, 2010. Biogeochemical study of a coccolithophore bloom in the northern Bay of Biscay (NE Atlantic Ocean) in June 2004. Prog. Ocean. 86, 317–336.

Holligan, P., Viollier, M., Harbour, D., Camus, P., Champagne-Philippe, M., 1983. Satellite and ship studies of coccolithophore production along a continental shelf edge. Nature 304, 339–342.

IOCCG, 2012. Ocean-Colour Observations from a Geostationary Orbit. Antoine D. (ed.), Reports of the International Ocean-Colour Coordinating Group, No. 12, IOCCG, Dartmouth, Canada.

Kotchenova, S.Y., Vermote, E.F., Matarrese, R., Klemm Jr, F.J., others, 2006. Validation of a vector version of the 6S radiative transfer code for atmospheric correction of satellite data. Part I: Path radiance. Appl. Opt. 45, 6762–6774.

Lutz, H., 1999. Cloud processing for meteosat second generation. EUMETSAT Tech Dep.

Nechad, B., De Cauwer, V., Park, Y., Ruddick, K., 2003. Suspended Particulate Matter (SPM) mapping from MERIS imagery. Calibration of a regional algorithm for the Belgian coastal waters. lQr 1, 52–0.

Nechad, B., Ruddick, K., Neukermans, G., 2009. Calibration and validation of a generic multisensor algorithm for mapping of turbidity in coastal waters, in: SPIE Europe Remote Sensing. p. 74730H–74730H.

Neil, C., Cunningham, A., McKee, D., Polton, J.A., 2012. Remote sensing of seasonal stratification dynamics in the southern Irish Sea. Remote Sens. Environ. 127, 288–297.

Neukermans, G., 2012. Optical in situ and geostationary satellite-borne observations of suspended particles in coastal waters. Ph.D. dissertation, Université du Littoral Côte d'Opale, France. Academic and Scientific Publishers, Brussels, Belgium Perma-links: http://www2.mumm.ac.be/downloads/publications/neukermans_phd_cover.pdf http://www2.mumm.ac.be/downloads/publications/neukermans_phd_manuscript_17x24.pdf.

Neukermans, G., Ruddick, K., Bernard, E., Ramon, D., Nechad, B., Deschamps, P.-Y., others, 2009. Mapping total suspended matter from geostationary satellites: a feasibility study with SEVIRI in the Southern North Sea. Opt. Express 17, 14029–14052.

Neukermans, G., Ruddick, K., Greenwood, N., 2012. Diurnal variability of turbidity and light attenuation in the southern North Sea from the SEVIRI geostationary sensor. Remote Sens. Environ. 124, 564–580.

Ruddick, K., Neukermans, G., Vanhellemont, Q., Jolivet, D., 2013. Challenges and opportunities for geostationary ocean colour remote sensing of regional seas: A review of recent results. Remote Sens. Environ.

Ruddick, K., Vanhellemont, Q., Yan, J., Neukermans, G., Wei, G., Shang, S., 2012. Variability of suspended particulate matter in the Bohai Sea from the geostationary Ocean Color Imager (GOCI). Ocean Sci. J. 47, 331–345.

Ryu, J.-H., Han, H.-J., Cho, S., Park, Y.-J., Ahn, Y.-H., 2012. Overview of geostationary ocean color imager (GOCI) and GOCI data processing system (GDPS). Ocean Sci. J. 47, 223–233.

Schmidt, S., Harlay, J., Borges, A., Groom, S., Delille, B., Roevros, N., Christodoulou, S., Chou, L., 2013. Particle export during a bloom of *Emiliania huxleyi* in the North-West European continental margin. J. Mar. Syst. 109, S182–S190.

Van der Woerd, H., Pasterkamp, R., 2004. Mapping of the North Sea turbid coastal waters using SeaWiFS data. Can. J. Remote Sens. 30, 44–53.

Vanhellemont, Q., Neukermans, G., Ruddick, K., 2013. Synergy between polar-orbiting and geostationary sensors: Remote sensing of the ocean at high spatial and high temporal resolution. Remote Sens. Environ.

Weeks, A., Simpson, J., Bowers, D., 1993. The relationship between concentrations of suspended particulate material and tidal processes in the Irish Sea. Cont. Shelf Res. 13, 1325–1334.

Wessel, P., Smith, W.H., 1996. A global, self-consistent, hierarchical, high-resolution shoreline database. J. Geophys. Res. 101, 8741–8743.

Wolff, W., Smit, C., 1990. The Banc d'Arguin as an environment for coastal waders. Ardea 78, 17–38.

Ziveri, P., Broerse, A.T., van Hinte, J.E., Westbroek, P., Honjo, S., 2000. The fate of coccoliths at 48 N 21 W, northeastern Atlantic. Deep Sea Res. Part II Top. Stud. Ocean. 47, 1853–1875.